# AN EXPERIMENTAL INVESTIGATION OF DROPLET FILM BOILING ON MACRO-ROUGHENED SURFACES

**Dudley J. Benton, Ph.D.**
**Department of Mechanical and Aerospace Engineering**
**University of Tennessee, Knoxville, Tennessee**

## ABSTRACT

Film boiling of individual drops on artificially macro-roughened surfaces was experimentally investigated. Film boiling on a smooth surface was also investigated in order to provide baseline data for computing heat transfer enhancement due to the macro-roughness. An improved method for determining heat transfer coefficients from experimental data are also presented.

## NOMENCLATURE

$A^*$ ..... dimensionless drop area ($A^*=A/\lambda^2$)
$A$ ..... vertically projected drop area
$h_D$ ..... drop heat transfer coefficient
$h_{fg}$ ..... latent heat of vaporization
$T_L$ ..... temperature of the liquid
$T_W$ ..... bulk surface temperature
$V$ ..... drop volume
$V^*$ ..... dimensionless drop volume ($V^*=V/\lambda^3$)
$\lambda$ ..... liquid/vapor interface length
$\rho_f$ ..... density of the liquid

## INTRODUCTION

Film boiling is usually defined as the mode of boiling that occurs when an essentially continuous layer of vapor separates the heating surface from the boiling liquid (Bromley, 1959). Because the thermal conductivity of a vapor is typically much less than the thermal conductivity of the liquid phase, the presence of a vapor layer between the heating surface and the boiling liquid generally results in heat transfer rates that are much lower than those associated with nucleate boiling phenomenon where the liquid is in direct contact with the heating surface. This phenomenon of film boiling can occur when the liquid is in a pool, flowing in a channel, or individual drops. This last configuration of drops undergoing film boiling is usually called Leidenfrost boiling (Bell, 1967) and is the subject of this investigation. Figure 1 shows a typical drop film boiling on a smooth surface.

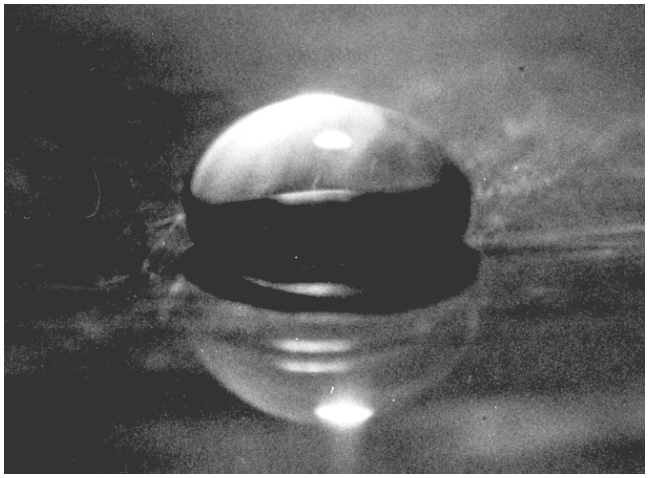

**Figure 1. Drop Film Boiling on a Smooth Surface**

An increase in film boiling heat transfer should result if direct contact between the heating surface and the boiling liquid were to be, if not to the degree associated with nucleate boiling, at least partially restored. It has been demonstrated experimentally (Bankoff and Mehra, 1962; Bradfield, 1966; Nishio and Hirata, 1978) that direct contact between the heating surface and the boiling liquid can occur in stable film boiling even on a smooth heating surface when vibration is present. With Leidenfrost drops in a gravitational field, the vapor, although less dense, is below the liquid, which gives rise to Taylor instabilities that can support wave-like disturbances at the liquid/vapor interface (Baumeister et al., 1977). Any disturbance of this liquid/vapor interface that might result from the introduction of the drop onto the heating surface or from ambient vibrations would increase the likelihood of contact with the surface. Liquid-solid contact is more likely to occur at the peaks on a rough surface. Figure 2 shows a drop film boiling on a grooved surface.

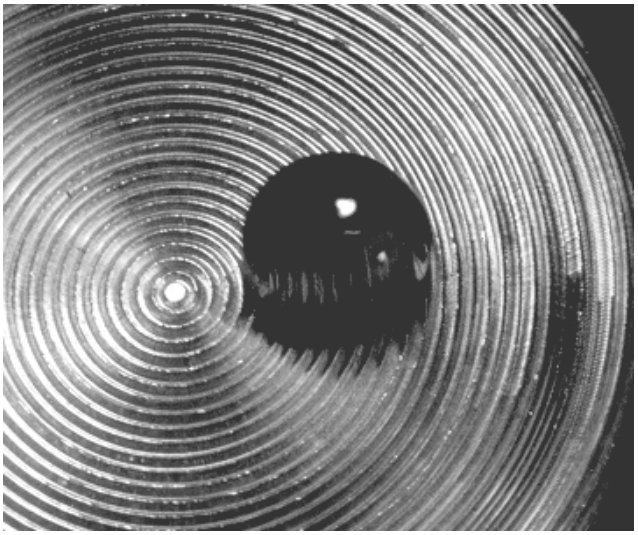

**Figure 2. Drop Film Boiling on a Grooved Surface**

When liquid-solid contact does occur the local heat flux and resulting vaporization of the liquid in the vicinity of contact is increased (Bradfield, 1966; Knobel and Yeh, 1977). This local increase in vaporization has two effects at the liquid-vapor interface: the interface may be pushed away from the heating surface and the interface is agitated. Even if the liquid-solid contact is broken, the agitation of the interface will increase the likelihood of contact elsewhere. Figure 3 shows a close-up of a drop film boiling above a surface with 0.165 cm diameter protruding cylindrical pins.

Several of studies (e.g., Bradfield, 1966; Nishio and Hirata, 1978; Tevepaugh and Keshock, 1979) indicate that most frequently in film boiling liquid-solid contact is of an intermittent rather than a continuous nature. Nishio and Hirata (who dealt with impinging rather than stationary drops) obtained photographic evidence that under certain circumstances, when the liquid comes into direct contact with the heating surface and the temperature of the surface at the point of contact is above some minimum value, rapid local vaporization will occur, causing the liquid to be lifted away from the surface at the point of contact, thus reestablishing the vapor layer

separating the heating surface from the boiling liquid. This local minimum temperature that must be maintained in order to subsequently maintain the vapor layer (that is characteristic of the film boiling phenomenon) is called the *local minimum film boiling temperature* (LMFBT). The bulk surface temperature required to maintain the LMFBT at every point on the heating surface where liquid-solid contact occurs is called the *bulk minimum film boiling temperature* (BMFBT).

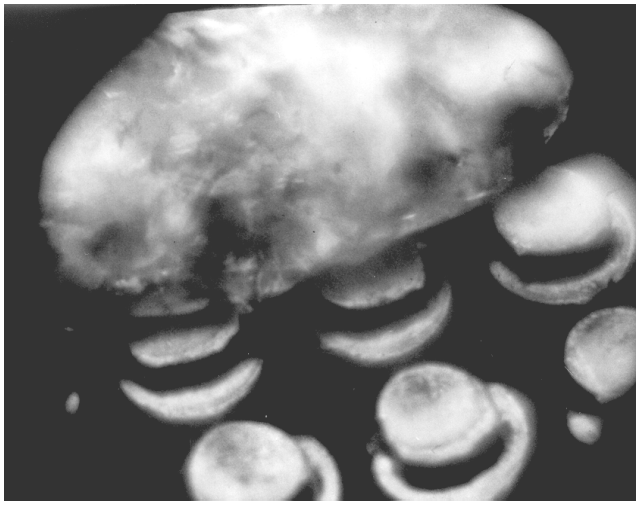

**Figure 3. Drop Film Boiling above 0.165 cm. Cylindrical Pins**

## EXPERIMENTAL APPARATUS AND PROCEDURE

### Liquids Investigated

The following four liquids were investigated: water, ethanol, isopropanol, and ethylene-chloride. These four liquids were chosen to provide a range of thermodynamic property values, molecular structure (polar/non-polar), and composition (inorganic/organic). The normal boiling point of the liquids ranged from 78.4°C (ethanol) to 100°C (water). Because the experiments were conducted under atmospheric conditions, liquids were chosen that had normal boiling temperatures in this range to minimize the heat transfer to or from the laboratory surroundings. The range of drop sizes investigated was approximately 0.01 cc. to 10 cc.

### Heating Surfaces

Five heating surfaces were investigated: a smooth surface for baseline comparison data (SMTH), two surfaces into which were machined concentric grooves (CG01 and SCG02), one surface which was drilled and into which were pressed cylindrical pins (CP54), and one surface into which were excavated diagonal slots forming right-hexagonal pins projecting from the surface (SHP2612). Surface SMTH, CG01, and CP54 were fabricated from mild steel, polished, and plated with nickel to inhibit corrosion. Surfaces SCG02 and SHP2612 were fabricated from type 321 stainless steel. The radial spacing of the grooves in surfaces CG01 and SCG02 were 0.051 cm. and 0.071 cm., respectively; and the depths were 0.020 cm. and 0.051 cm., respectively. Details of surface SCG02 are shown in Figure 4 and a close-up is shown in Figure 2. Surface CP54 was fabricated by drilling 0.165 cm. diameter holes on a 0.305 cm. center-to-center spacing and pressing cylindrical pins into the holes so that they protruded 0.152 cm. above the surface. A close-up of surface CP54 is shown in Figure 3. Surface SHP2612 was fabricated by milling three sets of 0.159 cm wide by 0.051 cm. deep slots having 0.305 cm. center-to-center spacing. The three sets of slots were cut at 30 degree angles, forming hexagonal pins of 0.051 cm. height, 0.146 cm. width, and 0.305 cm. center-to-center spacing. Details of surface SHP2612 are shown in Figure 5. The concentric grooves, cylindrical pin, and hexagonal pin geometries were selected simply for ease of fabrication.

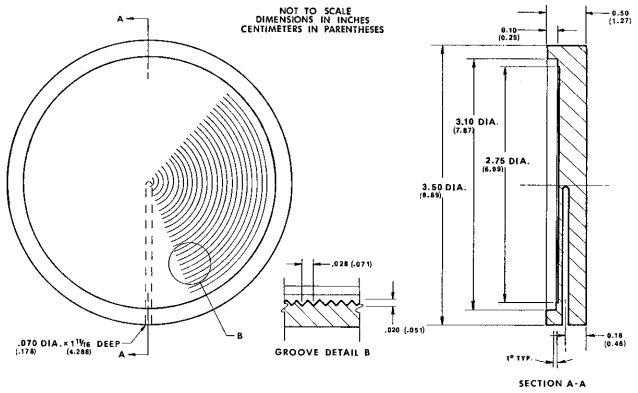


**Figure 4. Details of Surface SCG02**

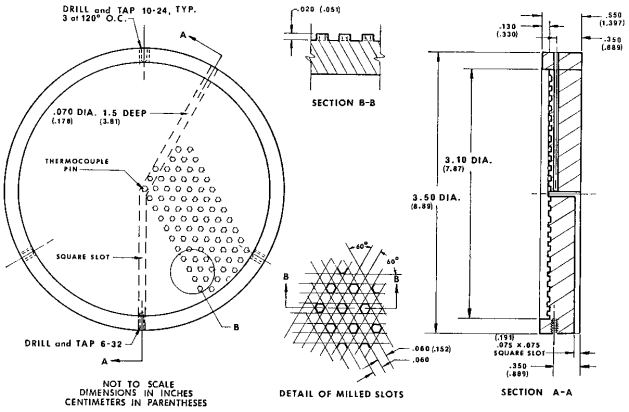


**Figure 5. Details of Surface SHP2612**

### Heating the Surfaces

The surfaces were heated from beneath by a gas burner or an electric hotplate. The maximum temperature that could be maintained by the hotplate was approximately 530°C. The data taken at bulk surface temperatures above 530°C utilized the gas burner. Surface temperatures were maintained throughout each data sequence by adjusting the rate of heat input. Several iterations were made at each condition in order to determine the required adjustment before any data were taken.

### Photography

The evaporating drops were photographed from above with a 16 mm single-frame camera. A mirror was suspended above the heating surface and at a 45-degree angle such that the horizontal lens of the camera was in view of the drop. The size of the drops was then determined from the photographs. The dimensions of the heating surface were used to determine the proper scale.

### Bulk Surface Temperature Measurements

The bulk temperature of the heating surfaces was determined from a chromel-alumel thermocouple inserted horizontally into the 0.178 cm diameter hole shown in Figure 4. The vertical temperature gradient within the heating surfaces (under the most extreme cases, based on

steady, one-dimensional conduction) was less than 120°C/cm over a distance of 0.24 cm; or a maximum temperature difference of 29°C. Because a vertical temperature gradient always exists in the heating surface by virtue of the heat being conducted to the boiling drops, no unique bulk surface temperature exists. In the present study, the characteristic bulk surface temperature was taken to be that indicated by the thermocouple that was located approximately in the center of the surface.

**Preparation of Heating Surfaces**

Although the heating surfaces were either nickel plated or high nickel stainless, some oxidation occurred. It was observed that the surfaces became discolored within a few minutes at high temperatures regardless of the polishing or cleaning prior to heating. After one hour above 500°C the oxide that formed on the surfaces appeared to remain relatively constant with time. Before each test, the surface was cleaned and then *seasoned* for one hour at 500°C before experiments were performed.

**Introduction of the Liquids to the Heating Surfaces**

In order to minimize the number of experimental variables, the liquids were heated to saturation prior to introduction to the heating surfaces. The liquids were introduced to the heating surfaces by gently pouring them from a beaker. The volume of the vaporizing drop at any particular time was determined from the photographs (in the manner which will be detailed subsequently). This technique of introducing the liquid to the heating surfaces minimizes three experimental variables typically associated with Leidenfrost film boiling data: (1) initial subcooling of the liquid, (2) initial drop volume, and (3) impingement velocity.

**Drop Area/Volume Calibration**

Known volumes of liquid, subcooled to minimize evaporation in transit, were gently poured onto the surfaces and several photographs taken at regular time intervals after deposition. The vertically projected drop area was determined from the photographs and was then extrapolated backward in time to the point when the drop was introduced to the surface. These area/volume data points were used to determine the value of the liquid/vapor interface parameter, $\lambda$ (Hartland and Hartley, 1976), that best related the drop area/volume data to the numerical solution to the Laplace capillary equation. The values of $\lambda$ determined in this manner were 0.219, 0.119, 0.0929, and 0.0889 cm for water, ethanol, isopropanol, and ethylene-chloride, respectively. Dimensionless drop profiles obtained by numerically solving the Laplace capillary equation are shown in Figure 6. Additional details are given in Appendix A.

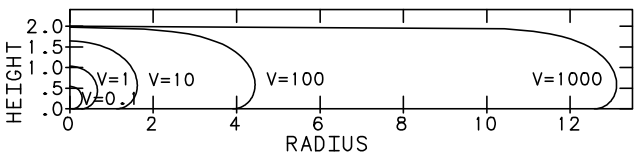


**Figure 6. Computed Dimensionless Drop Profiles**

The drop area/volume calibration points and the computed drop area/volume curve is shown in Figure 7. The numerical solution to the Laplace capillary equation and the respective value of $\lambda$ was used to determine the drop volume from the vertically projected drop area for each of the subsequent data points. No distinguishable difference in the drop area/volume relationship was noted on the macro-roughened surfaces as compared to the smooth surface. Data from all surfaces and liquids are shown together in Figure 7.

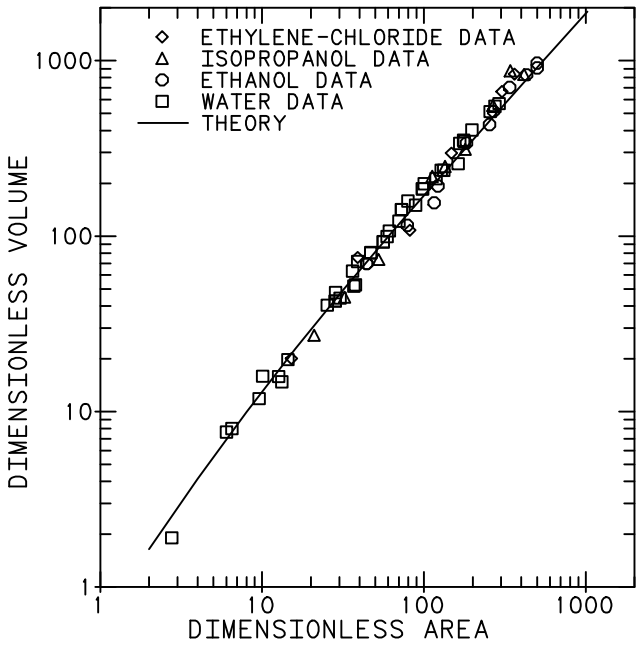


**Figure 7. Computed Dimensionless Drop Volume vs. Area**

**Determination of Heat Transfer Coefficients from Drop Area/Time Data**

The drop heat transfer coefficient as defined in the present study is given by Equation 1.

$$h_D = -\frac{\rho_f h_{fg} \dfrac{dV}{dt}}{A(T_W - T_L)} \qquad (1)$$

Thus the determination of heat transfer coefficients using Equation 1 necessitates the determination of the derivative of drop volume with respect to time from area/time data. Uncertainties in the experimentally measured area/time data will be increased by the differentiation process. The transformation of area/time data to volume/time data (through the numerical solution of the Laplace Capillary equation) will also result in an increased uncertainty. This procedure for determining heat transfer coefficients for Leidenfrost drops compounds the uncertainty of the data and thus the inconsistency between one set of data and another or between the data of one investigator and another. Baumeister and Schoessow (1969) show that this compounding of uncertainties can be greatly reduced by transforming Equation 1 and incorporating the definitions of dimensionless drop area and volume to obtain Equation 2.

$$h_D = -\frac{\lambda \rho_f h_{fg}}{(T_W - T_L)} \frac{dV^*}{dA^*} \frac{d\,[\ln(A)]}{dt} \qquad (2)$$

Mathematically, Equation 2 is equivalent to Equation 1. The dimensionless volume/area derivative, $dV^*/dA^*$, is also computed from the Laplace Capillary equation and is shown in Figure 8.

Experimental noise is introduced into the data due to uncertainties in the surface temperature, the timing of the photographs, and the projection and measurement of the drop areas. Noise is also added to the measured areas due to vibration of the drops. In addition to arising from deposition, these vibrations are thermally-driven and not easily eliminated. Baumeister, Hendricks, and Schoessow (1977) discuss these vibrations in detail. Accurately determining the time

derivative of the area must account for this noise in the data.

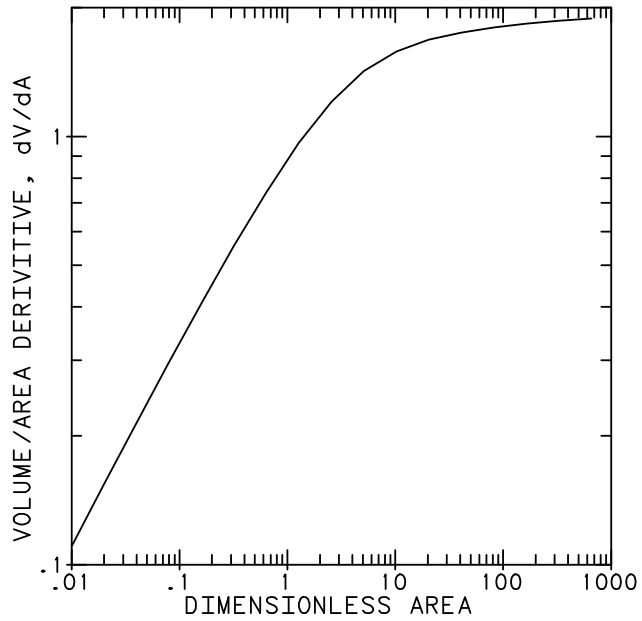


**Figure 8. Dimensionless Drop Area/Volume Derivative**

As the derivative of the natural log of the area is desired (see Equation 2), data reduction should focus on this quantity rather than the area itself. Some form of averaging or smoothening must be applied to minimize the effect of noise in the data, particularly the vibrations. A typical data sequence is shown in Figure 9. The shape of this evaporation curve on semi-log axes is typical of film boiling for all of the liquids and surfaces investigated. One hundred and twenty-five such curves were experimentally determined in this study. This curve shape is well approximated by a quartic in time for the log of the area in the least-squares sense. The quartic is analytically differentiated to evaluate Equation 2. An example of the approximating quartic is also shown in Figure 9.

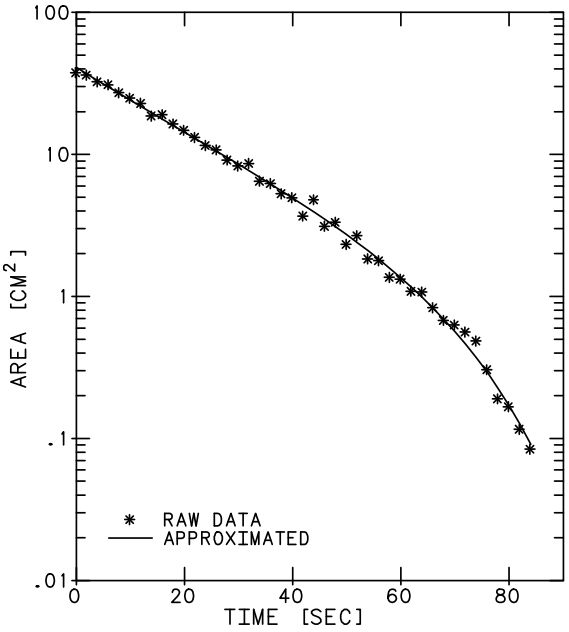


**Figure 9. Drop Area vs. Time**

## RESULTS

### Smooth Surface Data

The smooth surface (SMTH) data were taken to provide baseline data. The experimentally-determined heat transfer coefficient was compared to that obtained from the theoretical expression presented by Baumeister et al. (1966) and Baumeister et al. (1969) with a correction for higher vapor velocity and thermal gradient across the vapor layer. Details of the theoretical heat transfer coefficient for droplet film boiling on a smooth surface are given in Appendix B. The results for 29 evaporation sequences on the smooth surface are shown in Figure 10.

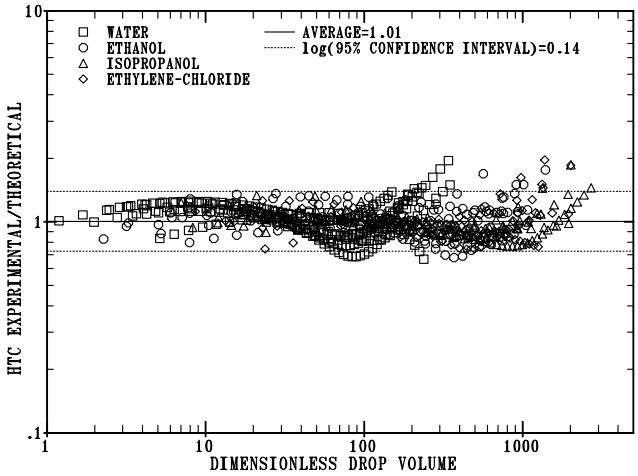


**Figure 10. Heat Trasnsfer on Smooth Surface**

Also shown on Figure 10 are the average (1.01) and the base-10 log of the 95% confidence interval (0.14). The net average error between the experimental and theoretical heat transfer coefficients on the smooth surface is then 1% (i.e., (1.01-1)*100). Ninety-five percent of the data lie within approximately 38% of this mean (i.e., $(10^{\pm 0.14}-1)*100$). These data indicate that the theoretical expression has an uncertainty (at the 95% percentile) of 38%, with negligible bias.

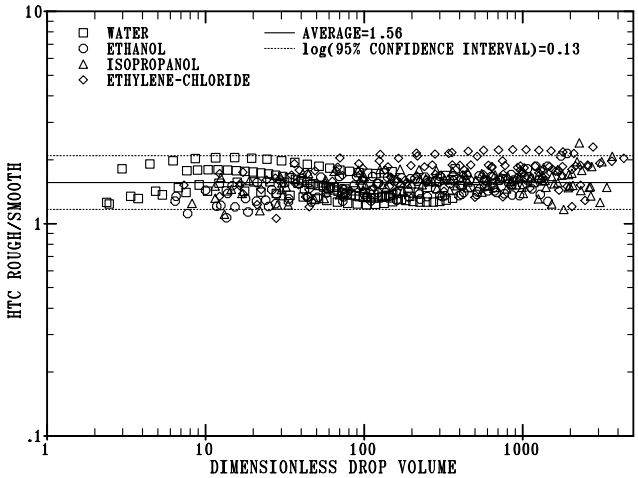


**Figure 11. Heat Transfer Enhancement on Surface CG01**

### Rough Surface Data

Data were also taken on the four macro-roughened surfaces. The rough surface data were divided by the theoretical smooth surface

heat transfer coefficient to obtain a normalized value. This would yield a ratio of 1 for no enhancement. There was no case in the present study where a decrease in heat flux was measured on a macro-roughened surface (i.e., all of the normalized rough surface heat transfer coefficients were greater than 1).

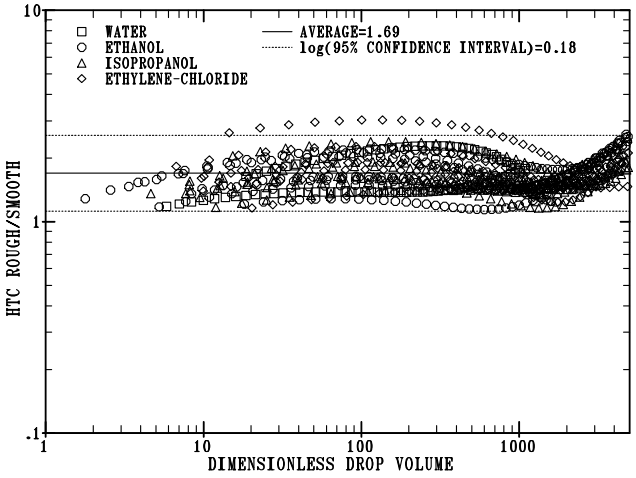


**Figure 12. Heat Transfer Enhancement on Surface SCG02**

The normalized heat transfer coefficients measured on the two grooved surfaces, CG01 and SCG02, are shown in Figures 11 and 12, respectively. The roughness of surface SCG02 is 39% higher than that of surface CG01 (0.071 vs. 0.051 cm.). The thermal conductivity of surface CG01 is approximately 3 times that of surface SCG02. The average heat transfer enhancements on these two surfaces are, as shown in the figures, 56% and 69%, respectively. Note that the base-10 log of the 95% confidence intervals are 0.13 and 0.18, respectively, which is on the same order as the confidence interval for the smooth surface data.

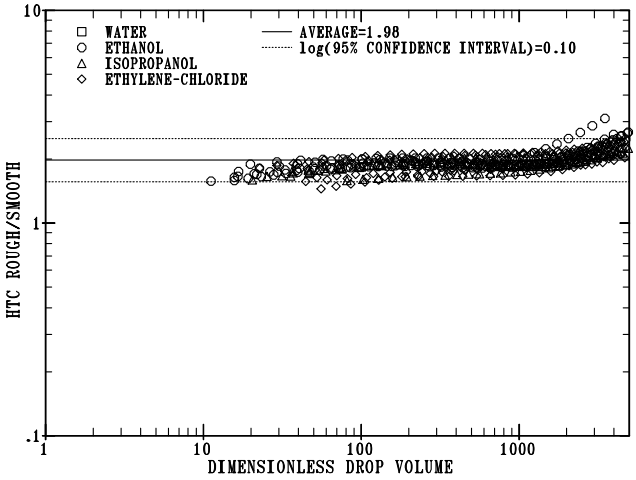


**Figure 13. Heat Transfer Enhancement on Surface CP54**

The normalized heat transfer coefficients measured on the two pinned surfaces, CP54 and SHP2612, are shown in Figures 13 and 14, respectively. The roughness of surface CP54 is almost three times that of surface SHP2612 (0.152 vs. 0.051 cm.). The thermal conductivity of surface CP54 is approximately 3 times that of surface SHP2612. The average heat transfer enhancements on these two surfaces are, as shown in the figures, 98% and 53%, respectively. Note that the base-10 log of the 95% confidence intervals are 0.10 and 0.15, respectively, which is on the same order as the confidence interval for the smooth and grooved surface data.

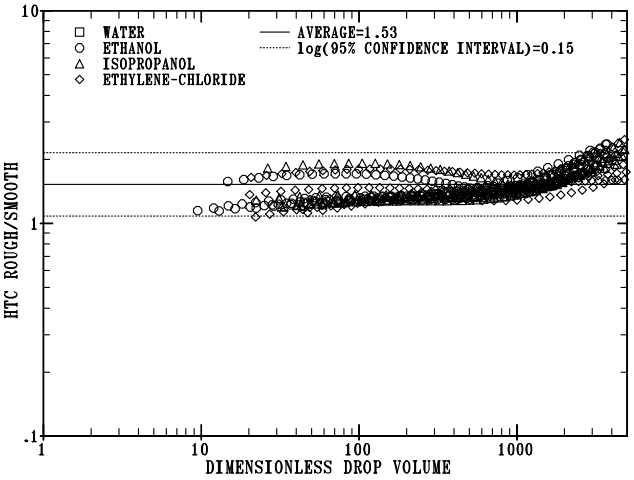


**Figure 14. Heat Transfer Enhancement on Surface SHP2612**

## CONCLUSIONS

Substantial increases in heat flux were measured on the macro-roughened surfaces (over that which was measured on the smooth surface). The relative increase in heat flux on the macro-roughened surfaces (as compared to the smooth surface) was seen to diminish with increasing surface temperature since the heat flux appears to increase with increasing liquid-solid contact and liquid-solid contact appears to increase with decreasing vapor layer thickness.

## REFERENCES

Bankoff, S. G., and V. S. Mehra, "A Quenching Theory for Transition Boiling," Industrial and Engineering Chemistry: Fundamentals, Vol. 1, No. 1, February 1962, pp 38-40.

Baumeister, K. J., and G. J. Schoessow, "Diffusive and Radiative Effects on Vaporization Times of Drops in Film Boiling," AICHE Symposium Series, Vol. 69, No. 131, 1969, pp 10-17.

Baumeister, K. J., T. D. Hamill, F. L. Schwarts, and G. J. Schoessow, "Film Boiling Heat Transfer to Water Drops on a Flat Plate," Proceedings of the Third International Heat Transfer Conference, Chicago, Illinois, August 1966.

Baumeister, K. J., R. C. Hendricks, and G. J. Schoessow, "Thermally Driven Oscillations and Wave Motion of a Drop," NASA TMX-73635, August, 1977.

Bell, K. J., "The Leidenfrost Phenomenon: A Survey," Chemical Engineering Progress Symposium Series, Vol. 63, No. 79, 1967, pp 74-85.

Benton, D. J., "Liquid-Solid Contact in Film Boiling of Leidenfrost Drops," Doctoral Dissertation, University of Tennessee, Knoxville, 1982.

Bradfield, W. S., "Liquid-Solid Contact in Stable Film Boiling," Industrial and Engineering Chemistry: Fundamentals, Vol. 5, No. 2, May 1966, pp 200-204.

Bromley, L. A., "Heat Transfer in Stable Film Boiling," Chemical Engineering Progress, Vol. 46, No. 5, May 1959, pp 221-227.

Hartland, S., and R. W. Hartley, Axisymmetric Fluid-Liquid Interfaces, Elsevier Scientific, Amsterdam, 1976.

Knobel, D. H., and Y. C. Yeh, "The Effect of Artificial Surface Projections on Film-Boiling Heat Transfer," Proceedings of the AICHE-ASME National Heat Transfer Conference, Salt Lake City, Utah, August 1977.

Leidenfrost, J. C., "On the Fixation of Water in Diverse Fire," trans. Carolyn Wares, International Journal of Heat and Mass Transfer, Vol. 9, November 1966, pp 1153-1166.

Nishio, S., and M. Hirata, "Direct Contact Phenomenon Between a Liquid Droplet and High Temperature Solid Surface," Proceedings of the Sixth International Heat Transfer Conference, Toronto, Canada, August 1978, pp 245-250.

Tevepaugh, J. A., and E. G. Keshock, "Influence of Artificial Surface Projections on Film Boiling Heat Transfer," Proceedings of the Eighteenth National Heat Transfer Conference: Advances in Enhanced Heat Transfer, San Diego, California, August 1979, pp 133-140.

**Appendix A: Capillary Equation for a Sessile Drop**

The Laplace capillary equation is discussed in detail by Hartland and Hartley (1976). The equations applicable to a sessile drop are as follows:

$$\frac{dr^*}{d\theta} = \frac{\cos\theta}{\frac{2}{b^*} + z^* - \frac{\sin\theta}{r^*}} \quad \textbf{(A1)}$$

$$\frac{dz^*}{d\theta} = \tan\theta \frac{dr^*}{d\theta} \quad \textbf{(A2)}$$

$$\frac{dV^*}{d\theta} = \pi r^{*2} \frac{dz^*}{d\theta} \quad \textbf{(A3)}$$

$$A^* = \pi r_{\max}^{*2} \quad \textbf{(A4)}$$

$$r^* = \frac{r}{\lambda} \quad \textbf{(A5)}$$

$$z^* = \frac{z}{\lambda} \quad \textbf{(A6)}$$

$$\lambda^2 = \frac{\sigma}{g(\rho_f - \rho_g)} \quad \textbf{(A7)}$$

$$b^* = \frac{1}{\lambda^2} \frac{dz^2}{d\theta^2}\bigg|_{\theta=0} \quad \textbf{(A8)}$$

Where $r$ is the radial distance from the centerline, $z$ is the vertical distance downward from the apex, $\theta$ is the angle of declination from the horizontal, $A^*$ is the dimensionless area, $V^*$ is the dimensionless volume, $\lambda$ is the interface length parameter, $\sigma$ is the surface tension, $g$ is the gravitational acceleration, $\rho_f$ is the density of the liquid (fluid), $\rho_g$ is the density of the vapor (gas), and $b^*$ is the dimensionless curvature at the apex. Further details are given by Benton (1982).

**Appendix B: Theoretical Heat Transfer Coeffient for Droplet Film Boiling on a Smooth Surface**

Baumeister, Hamill, Schwarts, and Schoessow (1966) present a complete development of a theoretical model for droplet film boiling on a smooth surface. Baumeister and Schoessow (1969) refine this by adding terms for radiation and diffusion. These models assume a creeping flow of vapor beneath the drop and a linear temperature gradient through the vapor. First order corrections for these simplifications are added here to improve the accuracy.

$$\Omega = \frac{C_{Pg}(T_W - T_L)}{h_{fg}} \quad \textbf{(B1)}$$

$$\Phi = \frac{\sigma(T_W^4 - T_L^4)}{(T_W - T_L)} \quad \textbf{(B2)}$$

$$\delta = \left[\left(3 + \frac{9\Delta}{20\mu_g}\right)\frac{\Delta\mu_g A^2}{2\pi g\,\rho_g(\rho_f - \rho_g)V}\right]^{\frac{1}{4}} \quad \textbf{(B3)}$$

$$\Delta = \left(\frac{k_g}{F(B)} + \Phi\delta\right)\frac{(T_W - T_L)}{h_{fg}} \quad \textbf{(B7)}$$

$$B = \frac{\Delta C_{Pg}}{k_g} \quad \textbf{(B4)}$$

$$F(B) = \int_0^1 e^{\left[\frac{B}{2}(1-2x^3+x^4)\right]}\,dx \quad \textbf{(B5)}$$

$$h_D = \frac{B k_g}{\delta\Omega} \quad \textbf{(B6)}$$

Where $\Omega$ is the dimensionless superheat, $C_{Pg}$ is the specific heat of the vapor, $T_W$ is the temperature of the heating surface, $T_L$ is the temperature of the evaporating liquid, $\Phi$ is the contribution due to radiation, $\sigma$ is the Stefan-Boltzmann constant, $\delta$ is the thickness of the vapor layer, $\Delta$ is the dimensionless vapor layer thickness, $\mu_g$ is the dynamic viscosity of the vapor, $A$ is the vertically-projected drop area, $g$ is the gravitational acceleration, $\rho_f$ is the density of the liquid (fluid), $\rho_g$ is the density of the vapor (gas), $V$ is the drop volume, $k_g$ is the thermal conductivity of the vapor, $B$ is the dimensionless boiling number, $F(B)$ is the dimensionless thermal boundary layer integral, $h_{fg}$ is the latent heat of vaporization, and $h_D$ is the droplet heat transfer coefficient. Equations B3, B4, and B5 must be solved iteratively. Initial estimates of $B=\Omega$ and $\Delta=\Omega k_g/C_{Pg}$ can be used.

The term in Equation B3 begining with 9/20 is the first order correction to the simplification that the flow of vapor beneath the drop is creeping (i.e., dominated by viscous effects). The function $F(B)$ is the first order correction to the simplification that the temperature gradient in the vapor is linear. Further details are given by Benton (1982).